Available online at www.sciencedirect.com
ScienceDirect
Trans. Nonferrous Met. Soc. China 29(2019) 2252−2261
Transactions of Nonferrous Metals Society of China
www.tnmsc.cn

Deformation characteristics and strain-compensated constitutive equation for AA5083 aluminum alloy under hot compression

Qing-song DAI[1,2], Yun-lai DENG[1], Jian-guo TANG[1], Yu WANG[1]

1. School of Materials Science and Engineering, Central South University, Changsha 410083, China;
2. Guangxi Liuzhou Yinhai Aluminum Co., Ltd., Liuzhou 545006, China

Received 22 February 2019; accepted 7 July 2019

Abstract: The hot deformation behavior of AA5083 aluminum alloy was studied using isothermal compression tests with a Gleeble−3500 thermal simulator at strain rate of 0.01−10 s^{-1} and at temperature of 300−500 °C. The experimental results indicate that dynamic recrystallization (DRX) tends to occur at high strain rates and temperatures, and therefore the flow stress is decreased. To predict the flow behavior under different deformation conditions, a strain-compensated constitutive equation based on Arrhenius-type equation and Zener–Hollomon parameters was proposed. The flow stresses obtained from the constitutive equation are consistent with the experimental results. The average absolute relative error is only 4.52% over the entire experimental range, indicating that the proposed constitutive equation exhibits high prediction precision for the hot deformation behavior of AA5083 aluminum alloy.

Key words: hot deformation; AA5083; dynamic recrystallization; constitutive equation

---

1 Introduction

Aluminum alloys have the primary potential for lightweight structural application in transportation, architecture, and other fields [1,2]. Among these, non-heat-treatable aluminum alloy 5083 is preferred because of its adequate strength, excellent corrosion resistance, and good welding performance [3,4]. Hot rolling is an important processing method for aluminum alloys, transforming ingots into sheets at high rates and large deformations. The general process parameters, hot rolling temperature, strain rate, and strain significantly influence the microstructure evolution, and consequently, the properties of alloys [5,6]. To optimize the process parameters and material performance, the hot deformation behavior of aluminum alloys was extensively investigated. Numerous constitutive equations, such as the Johnson−Cook (J−C) [7,8], Zerilli−Armstrong (Z−A) [9,10], Arrhenius-type with Zener−Hollomon parameters (Z−H) [11], Fields−Backofen (F−B) [12], and artificial neural network (ANN) models were proposed and revised to predict the flow stress affected by microstructure evolution during hot deformation. CHEN et al [13] studied the hot deformation behavior of AA6026 aluminum alloy using conventional and modified J−C models and a strain-compensated Z−H model. They suggested that the strain-compensated Z−H model offers the highest accuracy, followed by the modified and conventional J−C models. LI et al [14,15] compared the predictive capability of the strain-compensated Z−H and modified Z−A models for the hot deformation behavior of AA7050 aluminum alloy. Their results indicated that the Z−A model requires fewer parameters; however, Z−H is more accurate. BAKTASH and MIRZADEH [12] proposed a modified F–B model for the dynamic softening behavior of AA7075 aluminum alloy. TOROS and OZTURK [16] and HAGHDADI et al [17] set up the corresponding models for the flow behavior of Al−Mg and A356 aluminum alloys, respectively, based on the ANN method, and their results show that ANN offers good reliability based on a comparison with a modified Z−H model. All these constitutive equations can be classified as phenomenological constitutive, physics-based, and ANN equations [18−20]. The physics-based equation is

---

Foundation item: Project (51474240) supported by the National Natural Science Foundation of China; Project (AA16380036) supported by the Science and Technology Major Project of Guangxi Autonomous Region, China; Project (2017BF20201) supported by the Scientific Research and Technology Development Program of Liuzhou City, China

Corresponding author: Jian-guo TANG; Tel: +86-13574814750; E-mail: jgtang@csu.edu.cn

DOI: 10.1016/S1003-6326(19)65131-9

mainly used to analyze the effect of microstructure evolution on macroscopic mechanical properties. The phenomenological constitutive equation is generally semi-theoretical and semi-empirical, and the ANN equation is a complex network of interconnected processing units [7,21,22]. As one type of phenomenological constitutive equation, the Arrhenius equation is widely utilized in engineering as it has few material constants and is easy to build and calibrate. Many Arrhenius-modified constitutive equations for aluminum alloys have been established, in which the influence of strain has been considered to improve the prediction accuracy. WU et al [23] built a comprehensive constitutive equation coupling flow stress with strain, strain rate, and deformation temperature for a new Al−Zn−Mg−Er−Zr alloy, and the average absolute relative simulation error was only 4.54% over the entire investigation range. LIAO et al [24] developed a new constitutive equation incorporating the effect of strain on material constants for three Al−Si−Mg alloys, and the correlation coefficients between the experimental and predicted stresses reached 99.49%. WANG et al [25] proposed a revised Arrhenius-type model to describe the flow behavior of Al−Cu−Li alloy over wide ranges of deformation temperatures and strain rates. GAN et al [26] presented a revised constructive description for 6063 aluminum alloy under hot working.

The hot deformation behavior and constitutive equations for the AA5083 aluminum alloy were also reported. HOSSEINIPOUR [27] studied the stress–strain rate curves of the AA5083 aluminum alloy at 440−460 °C and strain rates of 9.26×10^{-4}−9.26×10^{-3} s^{-1} using strain rate jump tests. OTEGI et al [28] developed an algorithm for multi-stage identification of constitutive parameters and applied this to AA5083 alloy at strain rates of 2×10^{-4}−2×10^{-3} s^{-1} at 500 °C. ZHANG et al [29] proposed a modified constitutive model for the AA5083 aluminum alloy deformed at 20−250 °C with strain rates of 0.001−0.1 s^{-1}. However, the reported experimental conditions were different from those of actual hot rolling, which is usually conducted at 300−500 °C and strain rates of 0.01−10 s^{-1}. Moreover, most current constitutive equations for the AA5083 aluminum alloy were built through thermal tensile simulation experiments. In such simulations, the stress state of the material is different from that under hot rolling during deformation [30,31]. Conversely, a constitutive equation developed through thermal compression is preferred for optimizing the hot rolling process.

In this study, a series of isothermal compression tests for the AA5083 aluminum alloy were conducted at strain rates of 0.01−10 s^{-1} and 300−500 °C. The corresponding microstructure evolution and flow stress behavior were analyzed, and a strain-compensated constitutive equation was proposed based on an Arrhenius-type equation and Zener–Hollomon parameters. The reliability of the constitutive equation was evaluated over the complete experimental range.

2 Experimental

The material used in this investigation was an industrial Al−Mg−Mn ingot with a chemical composition (wt.%) of 4.8Mg−0.5Mn−0.1Cr−0.3Fe−0.1Si−(Bal.)Al. The as-cast sample was initially homogenized at 420 °C for 2 h and at 510 °C for 10 h before air-cooling to room temperature. Cylindrical specimens with dimensions of 15 mm (height) × 10 mm (diameter) were machined from the homogenized material. Compression tests were performed on a Gleeble−3500 thermal simulator at 300−500 °C with intervals of 50 °C, and the strain rates were set at 0.01, 0.1, 1 and 10 s^{-1}. Prior to hot compression, all specimens were heated to the target compression temperatures with a heating rate of 10 °C/s and held at the testing temperature for 3 min to obtain a uniform and stable temperature. Figure 1 displays a schematic of the thermal compression process. A hot-compressed sample was obtained after compression testing. The height of the hot-compressed sample was reduced by 50% compared with the original test specimen and represents a total true strain of 0.7.

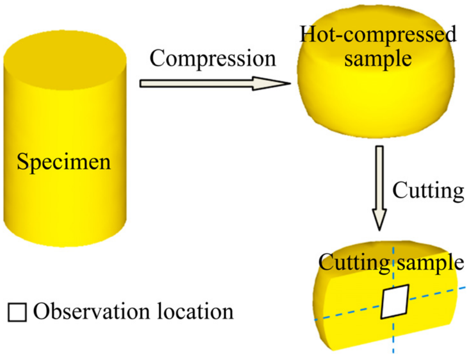

Fig. 1 Schematic of sample and process for compression microstructure examination

To study the effect of strain on microstructure evolution, two additional samples were compressed at 400 °C and a strain rate of 10 s^{-1}, with strains of 0.35 and 1.2. After hot compression, all samples were immediately quenched in cold water to maintain the deformation microstructure. As shown in Fig. 1, for microstructure observation, the hot-compressed sample was sectioned parallel to the longitudinal compression axis, and the sampling location was marked on the cut sample. Microstructural characterization was conducted by optical microscopy (OM, AXIO Scope A1 optical microscope) and transmission electron microscopy (TEM, FEI TecnaiG2 20). The OM specimens were polished and anode-coated at 20 V for 1 min using a solution of fluoroboric acid (10 mL) + water (400 mL). TEM samples were first mechanically ground and polished to less than 100 μm, punched into discs with a diameter of 3 mm, and finally twin-jet electropolished with an electrolyte solution of 30% nitric acid and 70% methanol at ~15 V DC below −25 °C.

3 Results and discussion

3.1 Deformation characteristics

Typical true stress–strain curves of the AA5083 aluminum alloy under different deformation conditions are shown in Fig. 2. During the early deformation stage, the flow stress increases rapidly with strain, and then attains gradually the peak at a strain of around 0.1. Thereafter, the curves achieve a quasi-steady state. Figure 3 presents the variation in flow stress against the temperature and strain rate at a true strain of 0.5. The effects of temperature and strain rate on the flow behavior of AA5083 alloy are clearly significant. The flow stress decreases from 120.8 to 19.4 MPa when the temperature increases from 300 to 500 °C at a strain rate of 0.01 s^{-1} ($\ln\dot{\varepsilon}$=−4.6). Moreover, it increases to 209.3 MPa when the strain rate changes from 0.01 s^{-1} ($\ln\dot{\varepsilon}$=2.3) to 10 s^{-1} ($\ln\dot{\varepsilon}$=2.3) at 300 °C. It is clear that the flow stress is negatively dependent on the deformation temperature but positively dependent on the strain rate.

Figure 4 shows bright-field TEM microstructures of samples compressed at 400 °C and a strain rate of 10 s^{-1} for strains of 0.35, 0.7 and 1.2. Figure 4(a) indicates that elongated deformed grains with a high density of tangled dislocations are the main microstructural features at a strain of 0.35. The stored energy increases with strain to provide sufficient driving force for migration of atoms and dislocations [32,33]. Consequently, the dislocation density decreases, and clear grain boundaries emerge, as shown in Figs. 4(b, c). The TEM images indicate that work hardening plays a dominant role at low strain, and then dynamic softening caused by dynamic recovery (DRV) and dynamic recrystallization (DRX) is activated with increasing strain [34,35]. Characterization of the TEM microstructure at different strains accounts for the variation in flow stress shown in Fig. 2, where flow stress first increases to a peak value due to work hardening with the formation of elongated grains and tangled dislocations, thereafter gradually increasing to a quasi-steady state owing to the competition between

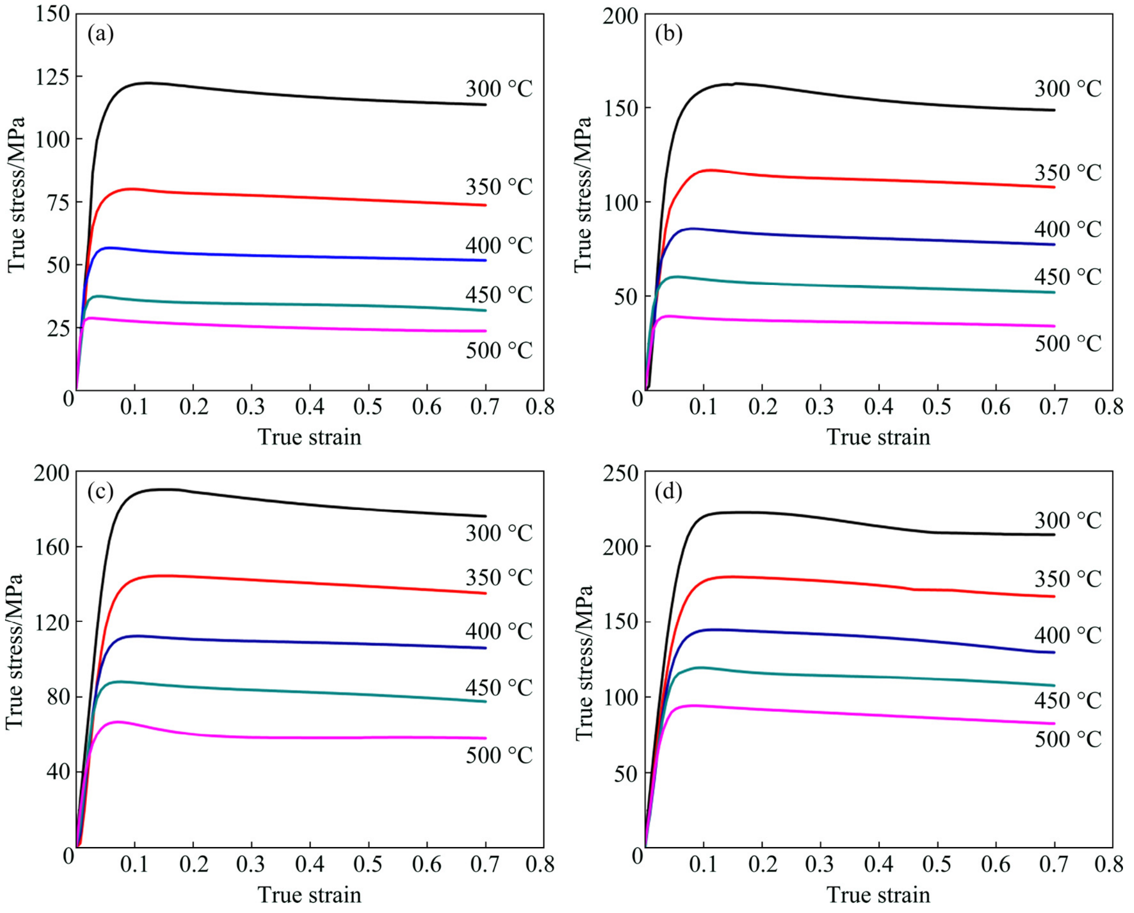

Fig. 2 True stress−strain curves of AA5083 aluminum alloy under different deformation conditions: (a) $\dot{\varepsilon}$=0.01 s^{-1}; (b) $\dot{\varepsilon}$ = 0.1 s^{-1}; (c) $\dot{\varepsilon}$ = 1 s^{-1}; (d) $\dot{\varepsilon}$ = 10 s^{-1}

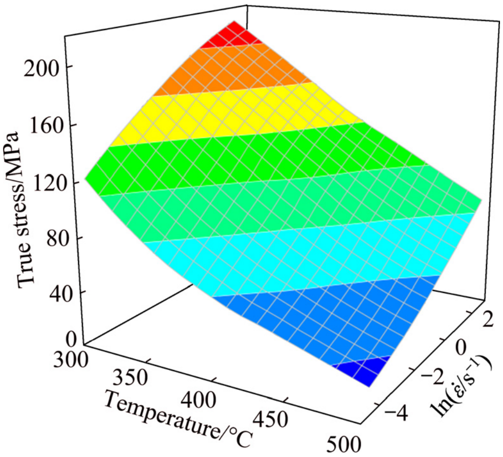

Fig. 3 Evolution of flow stress versus temperature and strain rate at strain of 0.5

work hardening and dynamic softening.

Figure 5 depicts the microstructure of AA5083 aluminum alloy compressed to a true strain of 0.7 under various hot deformation conditions. For comparison purposes, the original optical microstructure of the experimental material after homogenization treatment is also displayed in Fig. 5. As shown in Fig. 5(a), the original optical microstructure exhibits uniform equiaxed grains with an average grain size of 180 μm. The deformed grains are elongated after compression at a strain rate of 0.01 s^{-1} (see Fig. 5(b)). As the strain rate increases, recrystallized grains emerge and gradually increase, as shown in Figs. 5(c, d). It is apparent that the number and average size of the recrystallized grains increase with the deformation temperature by comparing the microstructures in Figs. 5(d, e, f). These features shown in Fig. 5 can be attributed to the following factors. Firstly, the stacking fault energy of aluminum alloy is high, and the deformation energy is easily released by DRV [36,37]. The increase in strain rate reduces the deformation time required for DRV to occur, resulting in the storage of deformation energy and the occurrence of DRX [38,39]. Simultaneously, the higher temperature reduces the resistance to dislocation movement and created suitable conditions for the DRX [38,39]. The microstructure evolution clarifies the flow stress trend shown in Fig. 3, where the flow stress increases with decreasing deformation temperature and increasing strain rate. The microstructural features are evidently closely related to the deformation parameters.

3.2 Constitutive modeling

To describe the relationships among flow stress, temperature, and strain rate under various deformation conditions for the AA5083 aluminum alloy, the Arrhenius constitutive equation and the Zener–Hollomon parameter (*Z*) in an exponent-type equation were employed [40,41]:

$$\dot{\varepsilon} = Af(\sigma)\exp[-Q/(RT)] \tag{1}$$

where

$$f(\sigma)=\begin{cases}\sigma^{n_1},\ \alpha\sigma<0.8\\ \exp(\beta\sigma),\ \alpha\sigma>1.2\\ \sinh(\alpha\sigma)^n,\ \text{for all } \sigma\end{cases} \tag{2}$$

$$Z=\dot{\varepsilon}\exp[Q/(RT)] \tag{3}$$

where $\dot{\varepsilon}$ is the strain rate (s^{-1}), σ is the flow stress (MPa), T is the absolute temperature (K), Q is the activation energy of hot deformation (kJ/mol), and R is the ideal gas constant (8.314 $J\cdot mol^{-1}\cdot K^{-1}$). A, n_1, n, α and β are material constants, and among them, $\alpha=\beta/n_1$.

As regards all the stress levels, Eq. (3) can be expressed as [11]

$$Z=A[\sinh(\alpha\sigma)]^n \tag{4}$$

Then, Eq. (4) is rewritten as

$$\sinh(\alpha\sigma)=(Z/A)^{1/n} \tag{5}$$

According to the definition of the hyperbolic sine function, it is easy to obtain

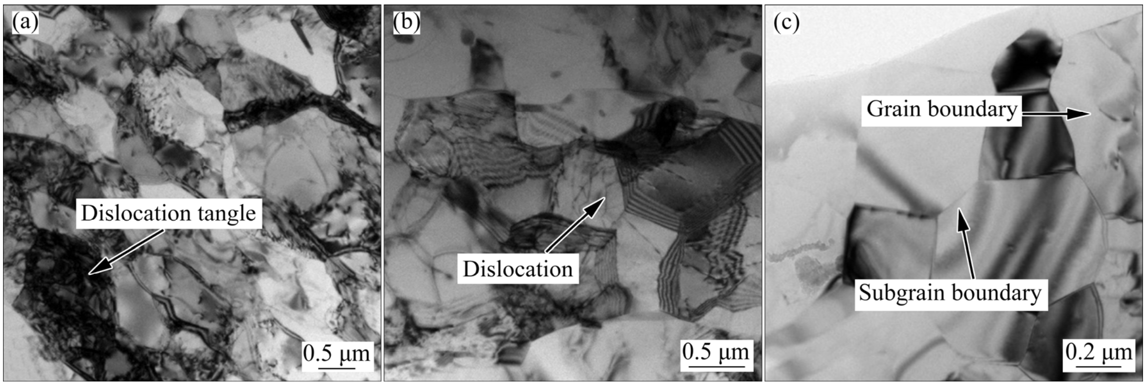

Fig. 4 TEM images of AA5083 aluminum alloy deformed at 400 °C and strain rate of 10 s^{-1} for different strains: (a) 0.35; (b) 0.7; (c) 1.2

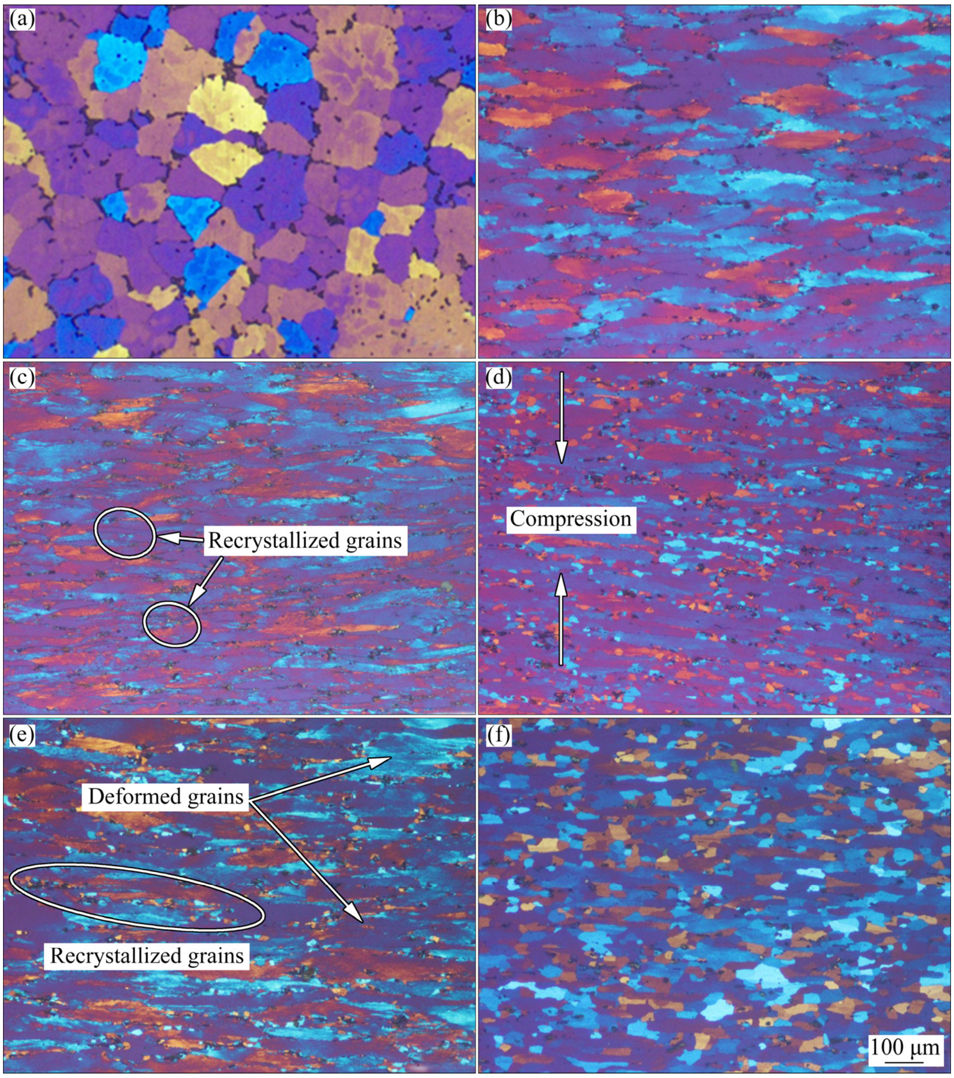

Fig. 5 Optical microstructures of AA5083 aluminum alloy under different deformation conditions: (a) Original; (b) 400 °C, 0.01 s^{-1}; (c) 400 °C, 1 s^{-1}; (d) 400 °C, 10 s^{-1}; (e) 300 °C, 10 s^{-1}; (f) 500 °C, 10 s^{-1}

$$\sinh^{-1}(\alpha\sigma)=\ln[(\alpha\sigma+\alpha\sigma^2+1)^{1/2}] \tag{6}$$

Combining Eqs. (5) and (6), the Arrhenius constitutive equation relating the flow stress to the Zener–Hollomon parameter can be expressed as follows:

$$\sigma=\frac{1}{\alpha}\{(Z/A)^{1/n}+[(Z/A)^{2/n}+1]^{1/2}\} \tag{7}$$

3.2.1 Determination of material constants for constitutive equation

To determine the material constants A, n_1, n, α and β, a true strain of 0.2 is employed as an example.

Substituting Eq. (2) into Eq. (1), and then taking the natural logarithms of both sides give

$$\ln\dot{\varepsilon}=\ln A_1-Q/(RT)+n_1\ln\sigma \tag{8}$$

$$\ln\dot{\varepsilon}=\ln A_2-Q/(RT)+\beta\sigma \tag{9}$$

$$\ln\dot{\varepsilon}=\ln A-Q/(RT)+n\ln[\sinh(\alpha\sigma)] \tag{10}$$

Substituting the flow stress at a true strain of 0.2 under different hot deformation conditions into Eqs. (8) and (9), as shown in Figs. 6(a, b), it is evident that the relationships $\ln\dot{\varepsilon}-\ln\sigma$ and $\ln\dot{\varepsilon}-\sigma$ can be well fitted by straight lines. The values of n_1 and β can be obtained from the mean slopes of the lines in Figs. 6(a) and (b), respectively. Thus, n_1=7.579, β=0.0819 MPa^{-1}, and α=0.0108 MPa^{-1}.

For a given strain rate, the activation energy Q can be obtained by differentiating Eq. (10):

$$Q=1000R\left\{\frac{\partial\ln[\sinh(\alpha\sigma)]}{\partial(1/T)}\right\}_{\dot{\varepsilon}}\left\{\frac{\partial\ln\dot{\varepsilon}}{\partial\ln[\sinh(\alpha\sigma)]}\right\}_{T}=RSn \tag{11}$$

with

$$\begin{cases} S=\left\{\dfrac{\partial\ln[\sinh(\alpha\sigma)]}{\partial(1/T)}\right\}_{\dot{\varepsilon}} \\ n=\left\{\dfrac{\partial\ln\dot{\varepsilon}}{\partial\ln[\sinh(\alpha\sigma)]}\right\}_{T} \end{cases} \tag{12}$$

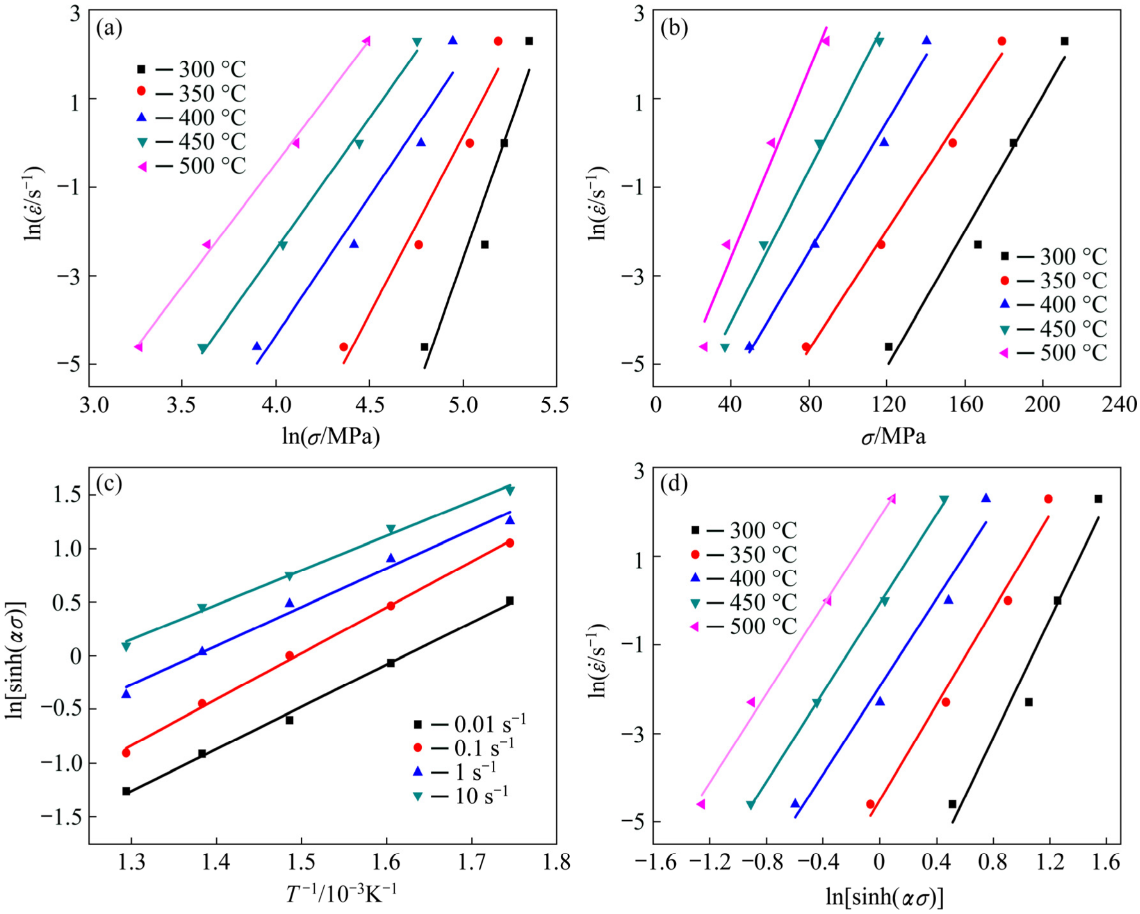

Fig. 6 Linear relationship fits: (a) $\ln\dot{\varepsilon}-\ln\sigma$; (b) $\ln\dot{\varepsilon}-\sigma$; (c) $\ln[\sinh(\alpha\sigma)]-1/T$; (d) $\ln\dot{\varepsilon}-\ln[\sinh(\alpha\sigma)]$

where S is the mean slope of $\ln\dot{\varepsilon}-\ln[\sinh(\alpha\sigma)]$ at various temperatures and n is the mean slope of $\ln[\sinh(\alpha\sigma)]-1/T$ at different strain rates, as shown in Figs. 6(c) and (d); n and S were calculated as 3.856 and 5.295, respectively. The deformation activation energy (Q) is then easily evaluated from Eq. (1) to be 168.61 kJ/mol by averaging the values of Q at different strain rates.

Taking the natural logarithm of both sides of Eq. (4) gives:

$$\ln Z=\ln A+n\ln[\sinh(\alpha\sigma)] \tag{13}$$

The values of Z at different temperatures and strain rates can be evaluated by substituting Q into Eq. (3). The linear relationship between Zener–Hollomon parameter $\ln Z$ and $\ln[\sinh(\alpha\sigma)]$ is plotted in Fig. 7. The slope and intercept of the $\ln Z-\ln[\sinh(\alpha\sigma)]$ plot in Fig. 7 represent n and $\ln A$, so that n and A can be evaluated as 5.336 and 3.32×10^{12} s^{-1}, respectively. The relative difference between the n-values in Eqs. (12) and (13) is less than 1.5%.

The values of A, n, α and Q at a true strain of 0.2 are listed in Table 1. Substituting these values into Eqs. (4) and (7), the Arrhenius constitutive equation of the AA5083 aluminum alloy at a given strain that relates the flow stress to the Zener–Hollomon parameter can be expressed as

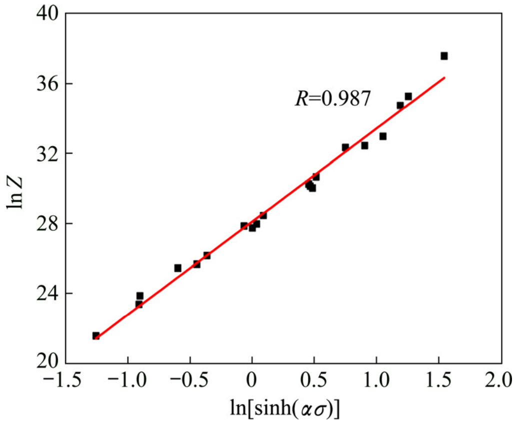

Fig. 7 Linear relationship between Zener–Hollomon parameter $\ln Z$ and $\ln[\sinh(\alpha\sigma)]$

$$\begin{cases}\sigma=\dfrac{1}{0.0108}\left\{\left[\left[\left(\dfrac{Z}{3.32\times10^{12}}\right)^{1/5.259}+\right.\right.\right. \\ \qquad\left.\left[\left(\dfrac{Z}{3.32\times10^{12}}\right)^{2/5.259}+1\right]^{1/2}\right\} \\ Z=\dot{\varepsilon}\exp\left(\dfrac{168610}{RT}\right)\end{cases} \tag{14}$$

Table 1 Values of material constants at strain of 0.2

α/MPa^{-1}	n	Q/(kJ·mol^{-1})	A/s^{-1}
0.0108	5.259	168.61	3.32×10^{12}

3.2.2 Strain compensation

It is widely acknowledged that the effect of deformation strain on the hot deformation flow behavior cannot be neglected [25,26]. As shown in Figs. 1 and 4, the flow stress and microstructure of the AA5083 aluminum alloy are different at various true strains. Therefore, it is evident that the true strain also significantly affects the activation energy (Q) and other material constants (α, β, n and ln A). However, the strain effects were not considered in the above equation. Therefore, strain compensation will be considered in the following calculation to derive a more precise constitutive equation.

The material constants (α, β, n, ln A and Q) of the constitutive equations, similar to the formula method at a strain of 0.2, were evaluated at strains ranging from 0.05 to 0.7 with interval of 0.05. It is clear that the relationship between strain and material constants is complex, as shown in Fig. 8, which indicates that the influence of strain cannot be neglected. Based on the calculation, the relationship between strain and material constants can be fitted by a 7th order polynomial, as shown in Eq. (15), and the corresponding polynomial fits of material constants for the AA5083 aluminum alloy are listed in Table 2. Then, a more precise Arrhenius constitutive equation with a strain compensation for the AA5083 aluminum alloy can be rewritten as Eq. (16), which accurately predicts the flow stress at strain rates of 0.01−10 s^{-1}, 300−500 °C, and true strains below 0.7. Usually, the deformation mechanism can be analyzed

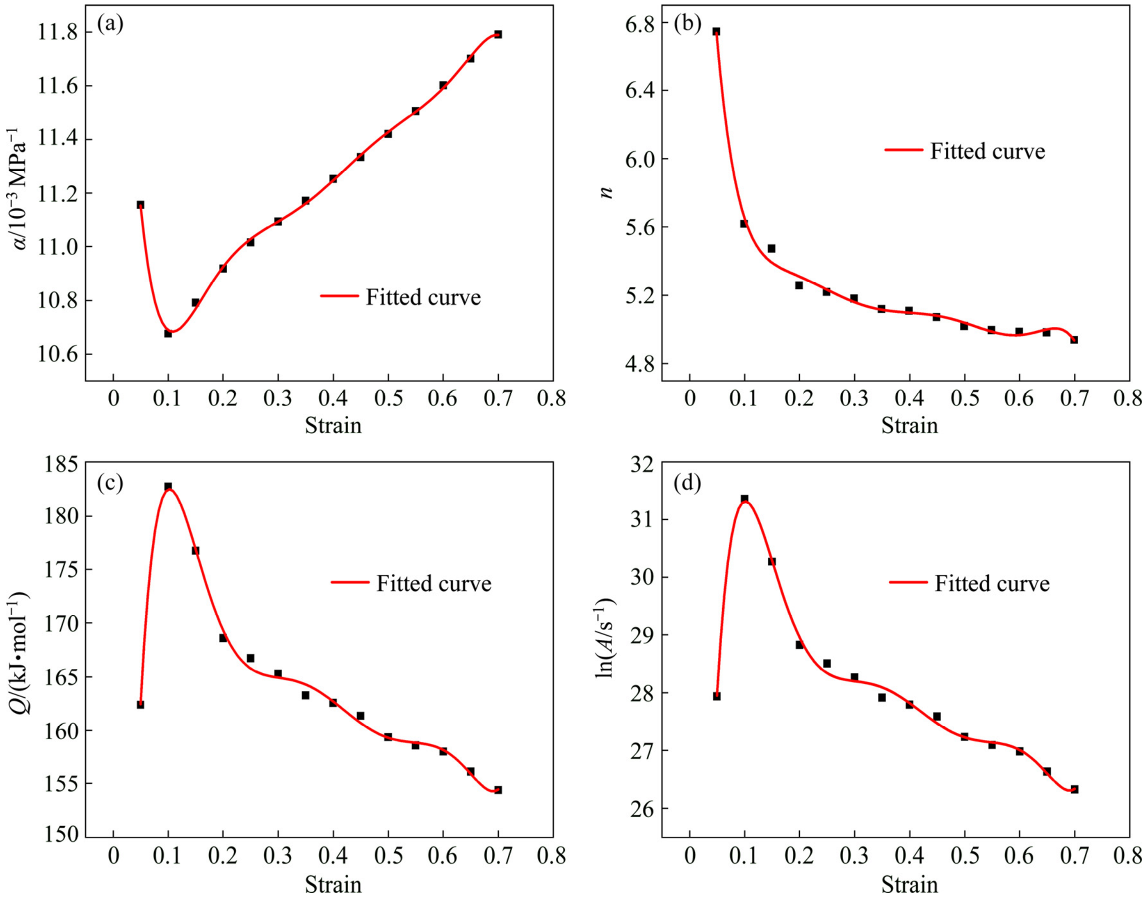

Fig. 8 Relationships between material constants (α, n, Q and ln A) and true strain by polynomial fit of AA5083 aluminum alloy

Table 2 Coefficients of polynomial fits for α, n, Q and ln A in Eq. (15) for AA5083 aluminum alloy

Parameter	B_0	B_1	B_2	B_3	B_4	B_5	B_6	B_7
$10^3\alpha$	13.27	−71.12	740.13	−3789.88	10789.79	−17332.70	14698.56	−5114.77
n	10.09	−106.18	1001.31	−5068.60	14627.81	−24062.71	20963.95	−7495.05
Q	59.8	3511.53	−37684.49	196180.57	−560814.77	898736.86	−757277.23	261138.75
ln A	10.3	605.78	−6536.18	34133.66	−97783.32	156953.65	−132425.86	45719.76

using the stress exponent (n) and activation energy (Q). The value of n is close to 5 and the average value of Q is 164 kJ/mol in this study (as shown in Figs. 8(b, c), which indicates that the main deformation mechanism is glide/climb-controlled dislocation creep caused by self-diffusion [42,43].

$$Y_{(\varepsilon)}=B_0+B_1\varepsilon+B_2\varepsilon^2+B_3\varepsilon^3+B_4\varepsilon^4+B_5\varepsilon^5+B_6\varepsilon^6+B_7\varepsilon^7 \tag{15}$$

$$\begin{cases}\sigma_{(\varepsilon)}=\dfrac{1}{\alpha(\varepsilon)}\left\{\left(\dfrac{Z}{A_{(\varepsilon)}}\right)^{\frac{1}{n_{(\varepsilon)}}}+\left[\left(\dfrac{Z}{A_{(\varepsilon)}}\right)^{\frac{2}{n_{(\varepsilon)}}}+1\right]^{\frac{1}{2}}\right\} \\ Z=\dot{\varepsilon}\exp[Q_{(\varepsilon)}/(RT)]\end{cases} \tag{16}$$

3.2.3 Evaluation of constitutive equation

It is necessary to assess the accuracy and reliability of the constitutive equations using the strain compensation. The calculated value was obtained by substituting the calculated material constants into Eq. (16), as shown in Fig. 9. It is clear that the predicted values of flow stress calculated from Eq. (16) are consistent with the test data for the AA5083 aluminum alloy.

Moreover, the correlation coefficient (R') and average absolute relative error (*AARE*) were employed to further evaluate the precision of the established constitutive equation. The R' and *AARE* can be described by Eqs. (17) and (18), respectively. As shown in Fig. 10, the predicted and experimental values reflect a good linear relationship with an R' value of 98.7%. The *AARE* is calculated as only 4.52%, which indicates that the developed Arrhenius constitutive equation relating flow stress to the Zener–Hollomon parameter has high prediction precision.

$$R'=\frac{\sum_{i=1}^{N}(\sigma_{\mathrm{E}}^{i}-\bar{\sigma}_{\mathrm{E}})(\sigma_{\mathrm{C}}^{i}-\bar{\sigma}_{\mathrm{C}})}{\sqrt{\sum_{i=1}^{N}(\sigma_{\mathrm{E}}^{i}-\bar{\sigma}_{\mathrm{E}})^2}\sqrt{\sum_{i=1}^{N}(\sigma_{\mathrm{C}}^{i}-\bar{\sigma}_{\mathrm{C}})^2}} \tag{17}$$

$$AARE=\frac{1}{N}\sum_{i=1}^{N}\left|\frac{\sigma_{\mathrm{E}}^{i}-\sigma_{\mathrm{C}}^{i}}{\sigma_{\mathrm{C}}^{i}}\right|\times 100\% \tag{18}$$

where σ_{E}^{i} is the test flow stress, σ_{C}^{i} is the predicted flow stress obtained using Eq. (16), $\bar{\sigma}_{\mathrm{E}}$ is the mean value of σ_{E}^{i}, $\bar{\sigma}_{C}$ is the average value of σ_{C}^{i}, and N is the total number of data points applied in the study.

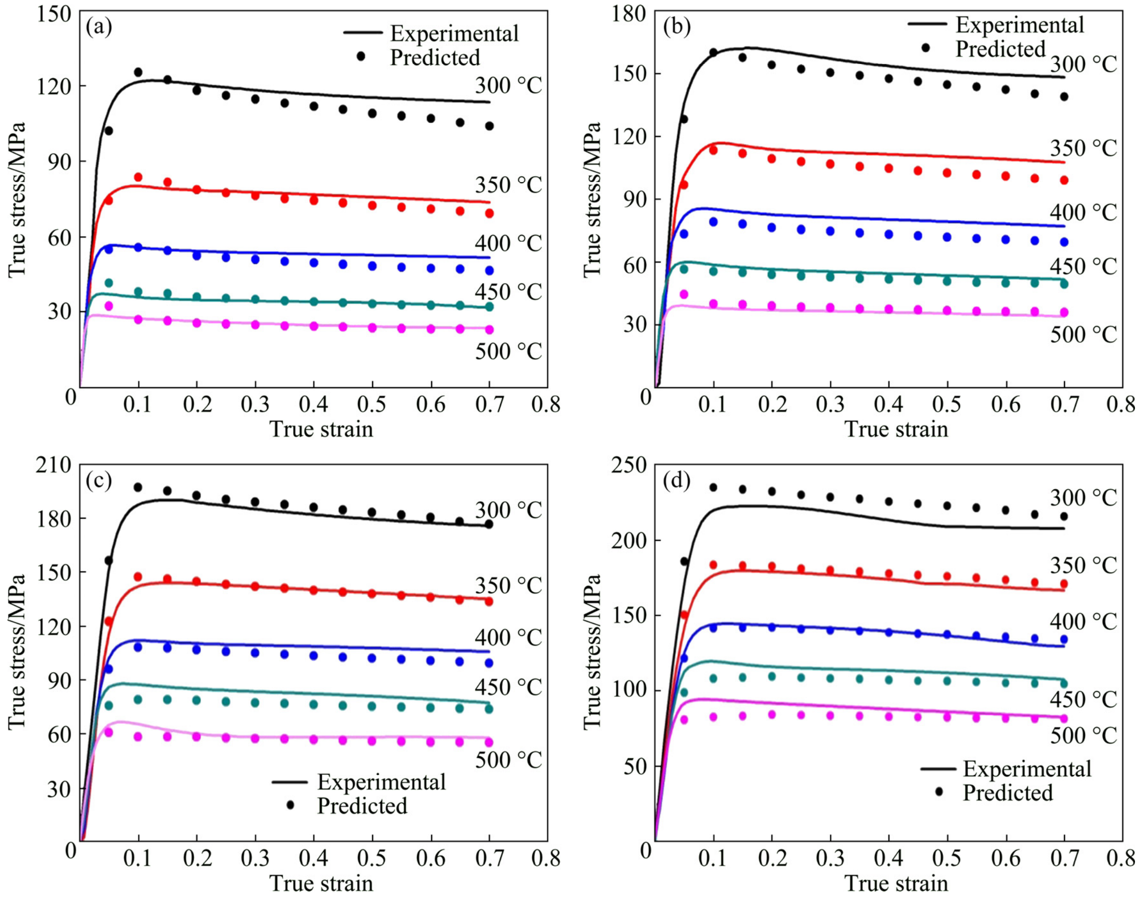

Fig. 9 Comparison between experimental and predicted flow stress curves of AA5083 aluminum alloy at different strain rates: (a) 0.01 s^{-1}; (b) 0.1 s^{-1}; (c) 1 s^{-1}; (d) 10 s^{-1}

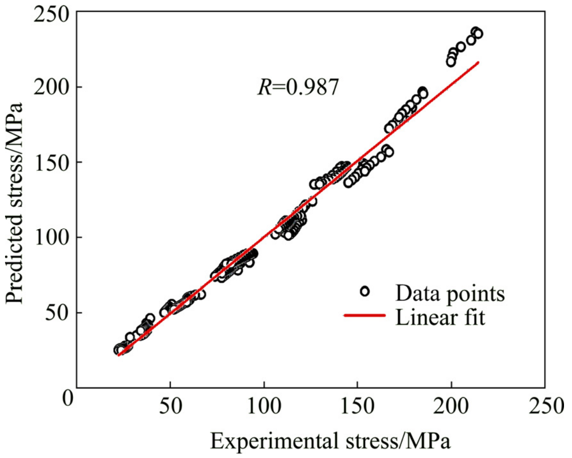

Fig. 10 Correlation between experimental and predicted flow stress obtained from constitutive equations

4 Conclusions

(1) DRX is more likely to occur at high strain rates and temperatures, decreasing flow stress. Hot deformation involves competition between work hardening and dynamic softening.

(2) A strain-compensated constitutive equation was proposed using an Arrhenius equation relating flow stress to the Zener–Hollomon parameter. The predicted flow stresses obtained from the established constitutive equation are consistent with the experimental results. The correlation coefficient (R) is 98.7% and the *AARE* is 4.52% over the entire experimental ranges, indicating that the proposed constitutive equation offers high prediction precision for the hot deformation behavior of the AA5083 aluminum alloy.

References

[1] GUO Xiao-bin, DENG Yun-lai, ZHANG Jin, ZHANG Xin-ming. A crystallographic orientation based model for describing the precipitation strengthening of stress-aged Al−Cu alloy [J]. Materials Science and Engineering A, 2015, 644: 358−364.

[2] JIRON-LAZOS U, CORVO F, de la ROSA S C, GARCIA-OCHOA E M, BASTIDAS D M, BASTIDAS J M. Localized corrosion of aluminum alloy 6061 in the presence of Aspergillus niger [J]. International Biodeterioration & Biodegradation, 2018, 133: 17−25.

[3] HUANG Yuan-chun, LI Yin, XIAO Zheng-bing, LIU Yu, HUANG Yu-tian, REN Xian-wei. Effect of homogenization on the corrosion behavior of 5083-H321 aluminum alloy [J]. Journal of Alloys and Compounds, 2016, 673: 73−79.

[4] ZHU Chen-xiao, TANG Xin-hua, HE Yuan, LU Feng-gui, CUI Hai-chao. Characteristics and formation mechanism of sidewall pores in NG-GMAW of 5083 Al-alloy [J]. Journal of Materials Processing Technology, 2016, 238: 274−283.

[5] KUMAR R V, KESHAVAMURTHY R, PERUGU C S, KOPPAD P G, ALIPOUR M. Influence of hot rolling on microstructure and mechanical behaviour of Al6061−ZrB_2 in-situ metal matrix composites [J]. Materials Science and Engineering A, 2018, 738: 344−352.

[6] ZHAO Qi, LIU Zhi-yi, LI Sha-sha, HUANG Tian-tian, XIA Peng, LU Lu-qing. Evolution of the Brass texture in an Al−Cu−Mg alloy during hot rolling [J]. Journal of Alloys and Compounds, 2017, 691: 786−799.

[7] MIRZADEH H. Constitutive modeling and prediction of hot deformation flow stress under dynamic recrystallization conditions [J]. Mechanics of Materials, 2015, 85: 66−79.

[8] AKBARI Z, MIRZADEH H, CABRERA J M. A simple constitutive model for predicting flow stress of medium carbon microalloyed steel during hot deformation [J]. Materials and Design, 2015, 77: 126−131.

[9] KOTUNDE N, KRISHNAMURTHY H N, PURANIK P, CUPTA A K, SINGH S K. Microstructure study and constitutive modeling of Ti−6Al−4V alloy at elevated temperatures [J]. Materials and Design, 2014, 54: 96−103.

[10] MIRZAIE T, MIRZADEH H, CABRERA J M. A simple Zerilli–Armstrong constitutive equation for modeling and prediction of hot deformation flow stress of steels [J]. Mechanics of Materials, 2016, 94: 38−45.

[11] MIRZADEH H. A simplified approach for developing constitutive equations for modeling and prediction of hot deformation flow stress [J]. Metallurgical and Materials Transactions A, 2015, 46: 4027−4037.

[12] BAKTASH R, MIRZADEH H. A simple constitutive model for prediction of single-peak flow curves under hot working conditions [J]. Journal of Engineering Materials and Technology, 2016, 138(021004): 1−5.

[13] CHEN Liang, ZHAO Guo-qun, YU Jun-quan. Hot deformation behavior and constitutive modeling of homogenized 6026 aluminum alloy [J]. Materials and Design, 2015, 74: 25−35.

[14] LI Jiang, LI Fu-guo, CAI Jun, WANG Rui-ting, YUAN Zhan-wei, XUE Feng-mei. Flow behavior modeling of the 7050 aluminum alloy at elevated temperatures considering the compensation of strain [J]. Materials and Design, 2012, 42: 369−377.

[15] LI Jiang, LI Fu-guo, CAI Jun, WANG Rui-ting, YUAN Zhan-wei, JI Guo-liang. Comparative investigation on the modified Zerilli–Armstrong model and Arrhenius-type model to predict the elevated-temperature flow behaviour of 7050 aluminium alloy [J]. Computational Materials Science, 2013, 71(3): 56−65.

[16] TOROS S, OZTURK F. Flow curve prediction of Al–Mg alloys under warm forming conditions at various strain rates by ANN [J]. Applied Soft Computing, 2011, 11(2): 1891−1898.

[17] HAGHDADI N, ZAREI-HANZAKI A, KHALESIAN A R. ABEDI H R. Artificial neural network modeling to predict the hot deformation behavior of an A356 aluminum alloy [J]. Materials and Design, 2013, 49: 386−391.

[18] PENG Jian, WANG Yong-jian, ZHONG Li-ping, PENG Long-fei, PAN Fu-sheng. Hot deformation behavior of homogenized Al−3.2Mg−0.4Er aluminum alloy, [J]. Transactions of Nonferrous Metals Society of China, 2016, 26: 945−955.

[19] REZAEI ASHTIANI H R, SHAHSAVARI P. A comparative study on the phenomenological and artificial neural network models to predict hot deformation behavior of AlCuMgPb alloy [J]. Journal of Alloys and Compounds, 2016, 687: 263−273.

[20] HUANG Chang-qing, DENG Jie, Wang Si-xu, LIU Lei-lei. A physical-based constitutive model to describe the strain-hardening and dynamic recovery behaviors of 5754 aluminum alloy [J]. Materials Science and Engineering A, 2017, 699(24): 106−113.

[21] BOBBILI R, RAMUDU B V, MADHU V. A physically-based constitutive model for hot deformation of Ti-10-2-3 alloy [J]. Journal of Alloys and Compounds, 2017: 696: 295−303.

[22] WANG S, LUO J R, HOU L G, ZHANG J S, ZHUANG L Z. Physically based constitutive analysis and microstructural evolution of AA7050 aluminum alloy during hot compression [J]. Materials

and Design, 2016, 107: 277−289.

[23] WU Hao, WEN Sheng-ping, HUANG Hui, WU Xiao-lan, GAO Kunyuan, WANG Wei, NIE Zuo-ren. Hot deformation behavior and constitutive equation of a new type Al−Zn−Mg−Er−Zr alloy during isothermal compression [J]. Materials Science and Engineering A, 2016, 651: 415−424.

[24] LIAO Heng-cheng, WU Yuan, ZHOU Ke-xin, YANG Jian. Hot deformation behavior and processing map of Al−Si−Mg alloys containing different amount of silicon based on Gleebe-3500 hot compression simulation [J]. Materials and Design, 2015, 65: 1091−1099.

[25] WANG Yong-xiao, ZHAO Guo-qun, XU Xiao, CHEN Xiao-xue, ZHANG Cun-sheng. Constitutive modeling, processing map establishment and microstructure analysis of spray deposited Al−Cu−Li alloy 2195 [J]. Journal of Alloys and Compounds, 2019, 779: 735−751.

[26] GAN Chun-lei, ZHENG Kai-hong, QI Wen-jun, WANG Meng-jun. Constitutive equations for high temperature flow stress prediction of 6063 Al alloy considering compensation of strain [J]. Transactions of Nonferrous Metals Society of China, 2014, 24: 3486−3491.

[27] HOSSEINIPOUR S J. An investigation into hot deformation of aluminum alloy 5083 [J]. Materials and Design, 2009, 30(2): 319−322.

[28] OTEGI N, GALDOS L, HURTADO I, LEEN S B. Analysis of the capabilities of a hyperbolic constitutive equation for Al-5083 superplastic aluminium alloy [C]// International Esaform Conference on Material Forming: Esaform. Belfast, 2011: 1574−1579.

[29] ZHANG Cun-sheng, XIE Fang-jie, YANG Ying, WANG Yu-bao. Identification of modified Swift constitutive model and its application in predicting FLDs of AA5083 at elevated temperatures [J]. Procedia Manufacturing, 2018, 15: 1142−1148.

[30] XIAO Wen-chao, WANG Bao-yu, WU Yong, YANG Xiao-ming. Constitutive modeling of flow behavior and microstructure evolution of AA7075 in hot tensile deformation [J]. Materials Science and Engineering A, 2018, 712: 704−713.

[31] LIN Yong-cheng, DING Yi, CHEN Ming-song, DENG Jiao. A new phenomenological constitutive model for hot tensile deformation behaviors of a typical Al−Cu−Mg alloy [J]. Materials and Design, 2013, 52(24): 118−127.

[32] LIN Yong-cheng, CHEN Ming-song, ZHONG Jue. Numerical simulation for stress/strain distribution and microstructural evolution in 42CrMo steel during hot upsetting process [J]. Computational Materials Science, 2008, 43(4): 1117−1122.

[33] QIN Xiao-yu, HUANG Da-wei, YAN Xiao-jun, ZHANG Xiao-yong, QI Ming-jing, YUE S. Hot deformation behaviors and optimization of processing parameters for alloy 602 CA [J]. Journal of Alloys and Compounds, 2019, 770: 507−516.

[34] ABBASSI F, SRINIVASAN M, LOGANATHAN C, NARAYANASAMY R, GUPTA M. Experimental and numerical analyses of magnesium alloy hot workability [J]. Journal of Magnesium and Alloys, 2016, 4(4): 295−301.

[35] ZANG Qian-hao, YU Hua-shun, LEE Y S, KIM M S, KIM H W. Hot deformation behavior and microstructure evolution of annealed Al−7.9Zn−2.7Mg−2.0Cu (wt.%) alloy [J]. Journal of Alloys and Compounds, 2018, 763: 25−33.

[36] ZHU Rui-hua, LIU Qing, LI Jin-feng, XIANG Sheng, CHEN Yong-lai, ZHANG Xu-hu. Dynamic restoration mechanism and physically based constitutive model of 2050 Al−Li alloy during hot compression [J]. Journal of Alloys and Compounds, 2015, 650: 75−85.

[37] CHIBANE N, AIT-AMOKHTAR H, FRESSENGEAS C. On the strain rate dependence of the critical strain for plastic instabilities in Al−Mg alloys [J]. Scripta Materialia, 2017, 130: 252−255.

[38] LI Dong-feng, ZHANG Duan-zheng, LIU Sheng-dan, SHAN Zhao-jun, ZHANG Xin-ming, WANG Qin, HAN Su-qi. Dynamic recrystallization behavior of 7085 aluminum alloy during hot deformation [J]. Transactions of Nonferrous Metals Society of China, 2016, 26: 1491−1497.

[39] CHEN Xi-hong, FAN Cai-he, HU Ze-yi, YANG Jian-jun, GAO Wen-li. Flow stress and dynamic recrystallization behavior of Al−9Mg−1.1Li−0.5Mn alloy during hot compression process [J]. Transactions of Nonferrous Metals Society of China, 2018, 28: 2401−2409.

[40] SELLARS C M, MCTEGART W J. On the mechanism of hot deformation [J]. Acta Metallurgica, 1966, 14(9): 1136−1138.

[41] LI Jiang, LI Fu-guo, CAI Jun. Constitutive model prediction and flow behavior considering strain response in the thermal processing for the TA15 titanium alloy [J]. Materials, 2018, 11: 1985.

[42] MIRZADEH H. Simple physically-based constitutive equations for hot deformation of 2024 and 7075 aluminum alloys [J]. Transactions of Nonferrous Metals Society of China, 2015, 25: 1614−1618.

[43] MIRZADEH H, ROOSTAEI M, PARSA M H, MADMUDI R. Rate controlling mechanisms during hot deformation of Mg−3Gd−1Zn magnesium alloy: Dislocation glide and climb, dynamic recrystallization, and mechanical twinning [J]. Materials and Design, 2015, 68: 228−231.

AA5083 铝合金热压缩变形行为及应变补偿本构方程

戴青松 1,2，邓运来 1，唐建国 1，王 宇 1

1. 中南大学 材料科学与工程学院，长沙 410083；2. 广西柳州银海铝业股份有限公司，柳州 545006

摘　要：采用 Gleeble−3500 热模拟试验机研究 AA5083 铝合金在应变速率 0.01~10 s^{-1}、变形温度 300~500 °C 条件下的热压缩变形行为。结果表明：该合金在高应变速率和高变形温度下容易发生动态再结晶，并引起流变应力下降。为了预测不同变形条件下的流动特性，建立基于 Arrhenius 型方程和 Zener−Hollomon 参数的应变补偿本构方程，本构方程预测值与实验结果吻合较好，在实验范围内两者的平均相对误差仅为 4.52%，说明提出的本构方程可对 AA5083 铝合金的热变形行为进行精确预测。

关键词：热变形；AA5083；动态再结晶；本构方程

(Edited by Bing YANG)